Eur. Phys. J. B (2024)97:46
https://doi.org/10.1140/epjb/s10051-024-00680-w

THE EUROPEAN PHYSICAL JOURNAL B

Regular Article - Solid State and Materials

Role of humidity and surface roughness on direct wafer bonding

B. N. J. Persson[1,2,a] and C. Mathew Mate[3,b]

[1] Peter Grünberg Institute (PGI-1), Forschungszentrum Jülich, 52425 Jülich, Germany
[2] MultiscaleConsulting, Wolfshovener Str. 2, 52428 Jülich, Germany
[3] SLAC National Accelerator Laboratory, Menlo Park, CA 94025, USA

Received 23 December 2023 / Accepted 20 March 2024
© The Author(s) 2024

Abstract. Bodies made from elastically stiff material usually bind very weakly unless the surfaces are flat and extremely smooth. In direct wafer bonding flat surfaces bind by capillary bridges and by the van der Waals interaction, which act between all solid objects. Here we study the dependency of the work of adhesion on the humidity and surface roughness in hydrophilic direct wafer bonding. We show that the long-wavelength roughness (usually denoted waviness) has a negligible influence on the strength of wafer bonding (the work of adhesion) from the menisci that form from capillary condensation of water vapor.

1 Introduction

Two neutral, elastically stiff and dry solid objects usually do not adhere to each other. This is a result of the surface roughness which reduces the area of real contact, where solid-solid adhesion can occur, to a very small fraction of the apparent area of contact. If a loading pressure is applied to increase this real contact area, the surface asperities are deformed storing up elastic energy at the interface, which is then given back when the loading pressure is released, resulting, in most cases, in a negligible adhesive force [1–5,7–10]. For extremely smooth surfaces (i.e., root-mean-square (rms) roughness $\lesssim 1$ nm), however, adhesion can be observed even for elastically stiff solids.

Here, we consider the case of hydrophilic direct wafer bonding, where adhesion occurs between the two surfaces, usually silicon wafers covered by thin SiO_2 oxide layers or silica glass surfaces (amorphous SiO_2). This process is initiated by capillary condensation of water vapor in the small gap between the surfaces that generates a sufficient capillary adhesion force to overcome the elastic repulsion once the loading pressure exceeds a certain threshold, leading to "interfacial collapse" where the real area of solid-solid contact suddenly increases [11,12].

For hydrophilic interfaces in a humid atmosphere, often the main contribution to the adhesion force comes from capillary bridges or menisci that form at the interface between the solids due to capillary condensation of water vapor [6,7,13–24]. In contrast no water capillary bridges form between hydrophobic surfaces, and the adhesive force, in the absence of covalent and ionic bonding, is mainly from the van der Waals interaction. This van der Waals adhesive force is usually much smaller than the capillary force for hydrophilic surfaces in a humid atmosphere.

For a perfectly smooth rigid sphere (radius R) in contact with a perfectly smooth flat surface, the pull-off force is given by Bradley equation $2\pi w_0 R$ (where w_0 is the work of adhesion) [25]. For a water capillary bridge (assuming complete wetting) $w_0 = 2\gamma \approx 0.17\ \mathrm{J/m^2}$ is twice the surface tension of water. For dry silica surfaces the van der Waals interaction gives $w_0 \approx 0.02 - 0.03\ \mathrm{J/m^2}$ so the pull-off force due to capillary adhesion is nearly ~ 10 times larger than obtained assuming only the van der Waals interaction.

Wafer bonding is strongly influenced by surface roughness. In most studies the surface roughness is only characterized by the root-mean-square (rms) roughness amplitude $h_{\rm rms}$, which is usually determined by the most long wavelength roughness components. We show that for wafer bonding the long wavelength roughness is unimportant. This result from the the existence of a roll-off region in the surface roughness power spectrum, separating the short wavelength ($\lesssim 60$ nm) roughness from the longer ($\gtrsim 30\ \mu$m) waviness roughness. As a result, to determine (or control) the strength of wafer bonding, the roughness needs to be determined only over the length scales up to 0.1 μm. Also, we show that a better measure than the rms-roughness of the potential strength of wafer bonding is the elasticity integral defined by (4) below.

[a] e-mail: b.persson@fz-juelich.de (corresponding author)
[b] e-mail: mathew.mate@comcast.net

2 Previous wafer bonding results

Wafer bonding is a topic of high practical importance and of great scientific interest, and many papers have been published about wafer bonding [26–34]. The strength of wafer bonding depends on the nature of the surface roughness which varies depending on the surface preparation method. Theory shows that the surface roughness on many length scales influence the work of adhesion, so it is not enough to characterize the surface with the rms roughness amplitude alone. For smooth surfaces like silicon wafers, the surface roughness on all relevant length scales can be studied using Atomic Force Microscopy (AFM). In addition, for strong bond formation the surfaces need to be cleaned and "activated". For silicon wafers two surface activation methods have been used: exposure to oxygen plasma or wet chemical surface activation.

Wafer bonding experiments use thin silicon disks with a diameter of order $\sim$ 10 cm and thickness $\sim$ 0.5 mm. When such disks are first brought into contact, the contact initially only occurs at asperity summits and a thin air film exists over most of the interface, which has to be squeezed out before atomic-scale contact can occur over the entire interface. If the applied pressure is uniform (e.g. from the gravity force on the upper disk), a very long time (several hours) may be needed before the solids make atomic contact. In practical applications, a squeezing force is applied at one point on the surface of the upper disk to nucleate an atomic contact region that then expands radially via interfacial collapse with a characteristic speed v that depends on the strength of the adhesive interaction. More exactly, if w is the work of adhesion (the energy per unit surface area to separate the surfaces), then a simple theory, where the resistance to squeeze-out of the air film is attributed to the viscous energy dissipation in the air film, predicts $v \propto w^{5/4}$ (see Ref. [35]). Due to the speed at which the contact zone propagates outward, there may not be enough time for the water to form the minimum free energy configuration.[1] Thus w may differ from the work of adhesion when this crack tip speed vanishes (which we denote by $w = w_0$, i.e., the work of adhesion at the minimum energy configuration). w_0 can also be measured using the cantilever bending testing methodology [see Fig. 17a]. In this study we will consider how w_0 depends on the surface roughness and the humidity for hydrophilic contact.

[1] Using the AFM tip-on-flat geometry in ambient conditions the formation of capillary bridges has been observed to occur on the ms time scale. Thus if an AFM tip is brought close to a wafer surface (of order Kelvin radius) it takes a few ms for a water bridge to nucleate and grow (the smaller the gap, the faster it is) [15]. For multi-contact interfaces it can take much longer for water layers, capillary bridges and friction/adhesion to reach steady state. In some cases the diffusion of water molecules in narrow gaps between two surfaces may play an important role [36]. In general, it is difficult to measure friction as a function of humidity without hysteresis. Thus to study the RH dependence of Si-on-Si interfaces, in Ref. [17] the RH was first lowered to almost 0 for an hour before increasing RH and equilibrating for an hour.

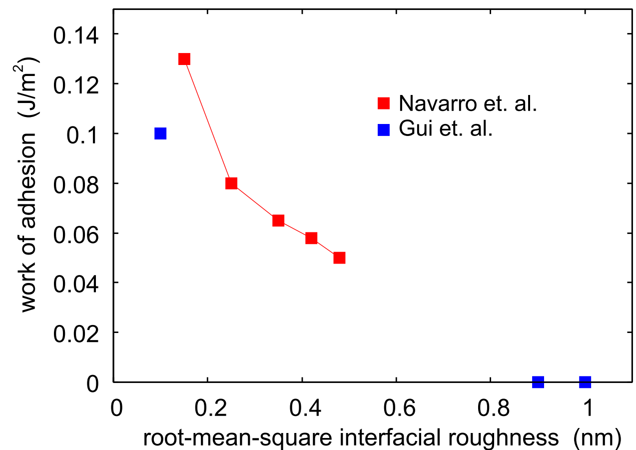

Fig. 1 The work of adhesion as a function of the root-mean-square (rms) roughness amplitude for silicon wafers with silicon oxide layers. Red squares are from Ref. [26] for the relative humidity RH = 0.4 and blue squares from Ref. [27] (unknown RH). The rms-roughness amplitudes was obtained from AFM topography measurements over 2 μm $\times$ 2 μm (Ref. [26]) and 10 μm $\times$ 10 μm regions (Ref. [27])

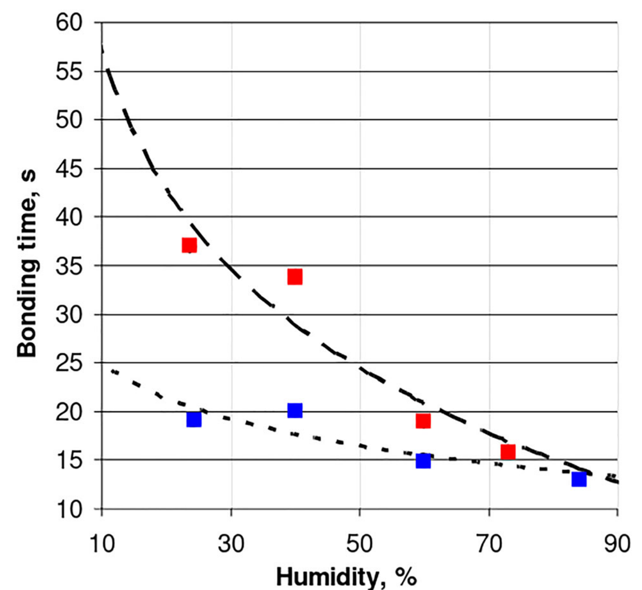

Fig. 2 Bonding time t_b as a function of humidity for wet chemical activated surfaces (red squares) and for plasma activated surfaces (blue squares). For silicon wafers bonding to glass surfaces. The work of adhesion is proportional to $t_b^{-5/4}$ (see Ref. [35]). From Ref. [28]

Figure 1 shows two sets of previously published experimental results that illustrate how the work of adhesion w_0 is a function of the root-mean-square (rms) roughness amplitude. The red squares are from Ref. [26] for the RH = 0.4 and was obtained from the bonding velocity assuming $w \propto v^{5/4}$. The blue squares are from

Ref. [27] (unknown RH) and was obtained using cantilever bending testing.

We note that, while the rms roughness amplitude generally depends on the size of the surface area studied, as we discuss below, the power spectra of silicon wafers typically have a roll-off region for roughness wavelength between 0.1 μm to a few μm so the rms roughness amplitude does not depend sensitively on the size of the studied region as long as it is in the roll-off region. For image sizes larger than ~ 10 μm the rms amplitude for wafers increases due to long wavelength roughness, usually referred to as waviness. As discussed below, this long wavelength roughness has only a small influence on the wafer bonding strength.

Figure 2 shows another set of previously published experimental results, which this time illustrate the importance of humidity to increasing the magnitude of the work of adhesion in hydrophilic wafer bonding. Figure 2 shows the bonding time $t_{\rm b}$ (the time it takes for the bonding wave to propagate throughout the whole nominal (final) contact region) as a function of humidity for silicon wafers bonding to glass surfaces [28]. The red squares are for wet chemical activated surfaces, and the blue squares for oxygen plasma activated surfaces. Assuming that the work of adhesion is proportional to $t_{\rm b}^{-5/4}$ (see Ref. [35]), we conclude that the work of adhesion then increases monotonically with increasing humidity. The different bonding times for the two cases studied cases may, in part, be due to different modifications of the surface topography by the chemical and oxygen plasma treatments.

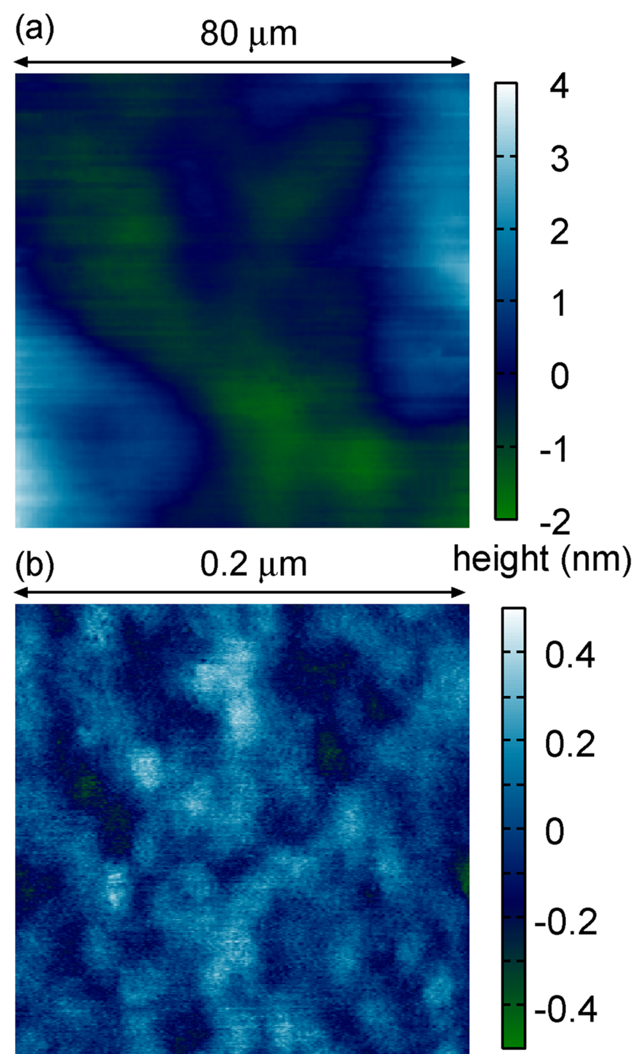

Fig. 3 AFM topography images of the Si(100) wafer over square areas of size **a** 80 μm $\times$ 80 μm and **b** 0.2 μm $\times$ 0.2 μm

3 Surface roughness power spectra

Many surfaces in nature have self-affine fractal surface roughness [37,38], i.e., when magnified, their roughness appears similar to the unmagnified surface, except that the amplitude of the roughness increases. The Hurst exponent H is a number between 0 and 1 which define the z-scaling factor needed in order for the magnified surface to appear similar to the unmagnified surface. $H = 1$ corresponds to a fractal-like surface where no scaling of the height coordinate is needed. Most self-affine fractal surfaces have $H > 0.7$ which can be explained using surface fragility arguments [38]. However, very smooth surfaces, such as surfaces with frozen capillary waves [5], may have $H < 0.5$.

Silicon wafers are very smooth and do not have self-affine fractal surface roughness, but have length-scale regions where the scaling properties are similar to self-affine fractal surfaces with $H \approx 0$ and $H \approx 1$ (Fig. 4).

For short ranged (contact) interaction theory shows that when $H > 0.5$ the long wavelength roughness has the strongest influence on the adhesion between solids while the opposite is true for $H < 0.5$ (see Ref. [1,3,4]). This is related to the elastic energy needed to deform the solids so they make contact in the nominal contact area. If this deformation energy is larger than the interfacial binding energy, resulting from the force field acting between the surfaces, no adhesion will be observed, as is the case for most elastically stiff solids unless the surfaces are extremely smooth. For surfaces that are not self-affine, such as the silicon wafers studied here, only a detail study can show if long-wavelength or short-wavelength roughness reduces the adhesion most. For such studies, which rely on the Persson theory of contact mechanics, the surface roughness power spectrum is of crucial importance [2,38–43].

The surface roughness power spectrum $C(q)$ is defined by

$$C(q) = \frac{1}{(2\pi)^2} \int d^2x \langle h(\mathbf{x}) h(\mathbf{0}) \rangle e^{-i\mathbf{q}\cdot\mathbf{x}} \qquad (1)$$

Here $z = h(\mathbf{x}) = h(x,y)$ is the surface height with the $z = 0$ plane chosen so that $\langle h \rangle = 0$, and $\langle .. \rangle$ stands for ensemble average, which in most cases is equivalent

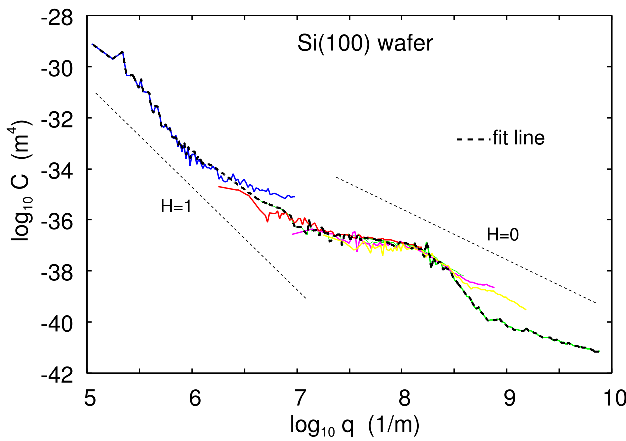

Fig. 4 The surface roughness power spectrum obtained from AFM topography data from a Si(100) wafer surface. The blue line was obtained from a 80 μm × 80 μm surface area, while the other curves was obtained from square areas with the side 0.2 (green line), 1 (yellow line), 2 (pink line) and 5 μm (red line). The dashed line is fitted to colored, experimental curves. The rms-roughness for the 80 μm surface is 0.95 nm and of the other surfaces 0.12, 0.14, 0.13, and 0.11 nm, respectively

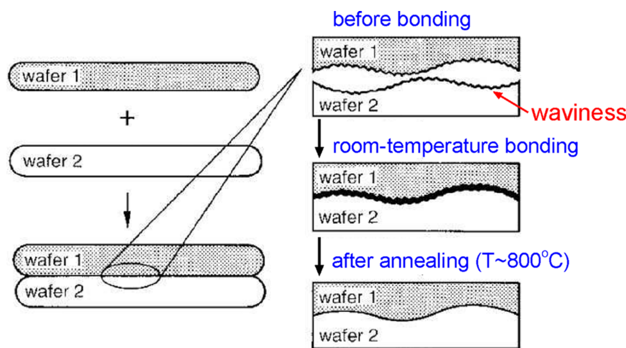

Fig. 5 The surface roughness on silicon wafers consist of two length scale regions, a long-wavelength region denoted “waviness” and short wavelength region extending down to atomic dimensions. During the initial wafer bonding (due to capillary bridges and the van der Waals interaction) the waviness deforms elastically and has only a small influence on the wafer bond strength. Strong chemical bonds form between the surfaces after a heat treatment

to averaging over the surface area. A self-affine fractal surface has a power spectrum $C(q) \sim q^{-2(1+H)}$. The root-mean-square (rms) roughness amplitude $h_{\rm rms}$ and the rms-slope ξ are easily calculated from the power spectrum using

$$h_{\rm rms}^2 = \langle h^2 \rangle = 2\pi \int_{q_0}^{q_1} dq\ qC(q) \quad (2)$$

$$\xi^2 = \langle (\nabla h)^2 \rangle = 2\pi \int_{q_0}^{q_1} dq\ q^3 C(q) \quad (3)$$

where q_0 and q_1 are the smallest and the largest roughness wavenumber included in the calculation.

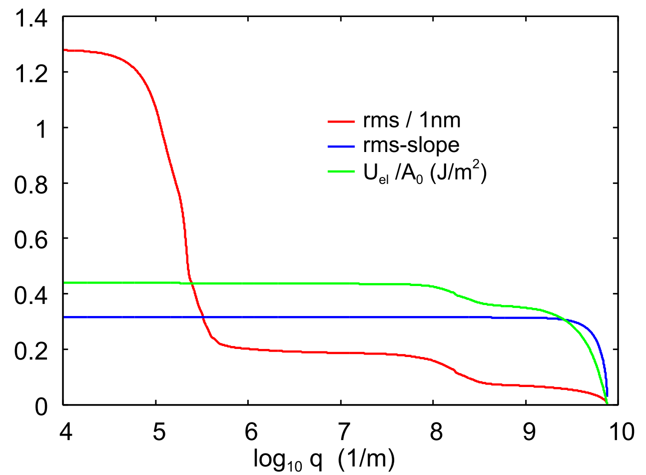

Fig. 6 The surface roughness rms amplitude (red line) in nm and the rms-slope (blue line) and the elastic energy per unit surface area assuming complete contact (green) in J/m^2, as a function of the low-wavenumber cut-off q for the wafer. In the calculation only the roughness components with wavenumber between q and the large-wavenumber cut-off q_1 (here $q_1 \approx 8 \times 10^9$ m^{-1}) is included, i.e. we use (2), (3) and (4) with q_0 replaced by q

Another important quantity is the elastic energy stored per unit surface area when two solids with the combined surface roughness power spectrum $C(q)$ are in complete contact:

$$\frac{U_{\rm el}}{A_0} = E^* \frac{\pi}{2} \int_{q_0}^{q_1} dq\ q^2 C(q) \quad (4)$$

where E^* is the effective Young's modulus (see below).

Here we are interested in very smooth surfaces such as highly polished glass surfaces or silicon wafers. Such surfaces have similar rms-roughness, typically of order 0.1 − 1 nm when studied over surface areas of linear size ∼ 1 μm, and similar forms of the surface roughness power spectra. In most cases the height probability distribution is nearly Gaussian.

3.1 AFM topography measurements

In the present study we use the surface roughness power spectrum obtained from atomic force microscopy (AFM) topography measurements on a Si(100) wafer. To obtain different magnitudes of the roughness, we scale the power spectrum with different prefactors. Note that since $C(q)$ is quadratic in $h(\mathbf{x})$ scaling the power spectrum with a factor s^2 correspond to scaling the rms-roughness amplitude with a factor s.

Using AFM we have measured the height topography of Si(100) wafers with square image sizes ranging from 0.2 μm×0.2 μm to 80 μm×80 μm, see Figs. 3 and 4. The blue line in Fig. 4 shows the surface roughness power spectrum obtained from the 80 μm×80 μm surface area, while the other curves was obtained from square areas with the side 0.2, 1, 2 and 5 μm. Figure 3 shows that

the Si(100) surface has (a) long wavelength waviness with wavelengths > 10 μm and (b) short wavelength roughness with a wavelength ~ 0.05 μm. In the power spectrum these two regions are separated by a roll-off region. We will show below that the long wavelength roughness has a negligible effect on the wafer bonding (see Fig. 5). Hence studying the surface roughness over small surface areas with the lateral size of order ~ 1 μm is enough for determining the strength of the capillary adhesion for wafer bonding in most cases.

Figure 6 shows the surface roughness rms-amplitude (red line) in nm, the rms-slope (blue line) and the elastic energy per unit surface area, $U_{\rm el}/A_0$, assuming complete contact (green) in J/m^2, as a function of the low-wavenumber cut-off q for the wafer. In the calculation only the roughness components with wavenumber between q and the large-wavenumber cut-off q_1 (here $q_1 \approx 8 \times 10^9$ m^{-1}) is included, i.e. we use (2)-(4) with q_0 replaced by q. The elastic energy $U_{\rm el}$ is proportional to the effective Young's modulus E^* [defined below after (5)], and we have used $E^* \approx 71.6$ GPa. Note the roll-off region between 10^6 m^{-1} $< q < 10^8$ m^{-1}, where the rms-roughness amplitude is nearly constant, which is also the roll-off region of the $C(q)$ curve. The figure also shows that the rms-slope is determined by the very shortest roughness wavelength component and that $U_{\rm el}/A_0$ is independent of the roughness in the roll-off region. The latter indicate that the roughness in the roll-off region is unimportant for the wafer bonding which is also confirmed by calculations below. This is opposite to most "normal" cases where it is the long wavelength roughness which kills adhesion [1]. This difference results from the peculiar form of the power spectrum of the wafer surface with the waviness region occurring at several decades longer wavelength than the (short wavelength) surface roughness region.

4 Theory and numerical results

In this section we first describe the theory used to study capillary adhesion. Next we present the numerical results focusing on the work of adhesion and the average surface separation, assuming that thermal (or kinetic) equilibrium with the water vapor phase occur at all stages during pull-off.

4.1 Theory

We will use the same theory for capillary adhesion as presented in Ref. [7] which we briefly review here. Consider the contact between two solids with the roughness profiles $z = h_1(\mathbf{x})$ and $h_2(\mathbf{x})$ and with the Young's elastic modulus and Poisson ratio (E_1, ν_1) and (E_2, ν_2), respectively. For relative smooth surfaces, where the average rms surface slopes are much smaller than 1 this problem is equivalent to a perfectly flat and rigid solid in contact with an elastic solid with the surface profile $z = h_1(\mathbf{x}) + h_2(\mathbf{x})$ and the effective Young's modulus E and Poisson ratio ν

$$\frac{1-\nu^2}{E} = \frac{1-\nu_1^2}{E_1} + \frac{1-\nu_2^2}{E_2} \tag{5}$$

We define the effective modulus $E^* = E/(1-\nu^2)$. The elastic properties of silicon are anisotropic but here we use an average modulus $E_1^* = 144$ GPa giving for silicon in contact with silicon $E^* = 72$ GPa. We note that silica has a modulus roughly half of that of silicon and that when the roughness on the two surfaces are uncorrelated the power spectrum of the combined roughness $h = h_1 + h_2$ is $C = C_1 + C_2$.

We assume that the solids are in contact in a humid atmosphere (water vapor pressure $P_{\rm v}$) and that thermal equilibrium occurs. For hydrophilic surfaces, capillary bridges form at the interface with a meniscus radius $r_{\rm K}$ given by the Kelvin equation

$$r_{\rm K} = -\frac{\gamma v_0}{k_{\rm B}T\ln(P_{\rm v}/P_{\rm sat})} \tag{6}$$

where v_0 is the volume of a water molecule in the liquid state. The height of the capillary bridge or meniscus

$$d_{\rm K} = r_{\rm K}\,(\cos\theta_1 + \cos\theta_2) \tag{7}$$

where θ_1 and θ_2 are the water contact angles on the two solid surfaces. In the water meniscus, a negative (Laplace) pressure acts with $p = -p_{\rm K}$ where $p_{\rm K} = \gamma/r_{\rm K}$. In what follows we assume complete wetting, $\theta_1 = \theta_2 = 0$. In this case $d_{\rm K} = 2r_{\rm K}$ and $p_{\rm K} = 2\gamma/d_{\rm K}$. We further assume that the Kelvin equation holds down to a Kelvin radius as small as $r_{\rm K} = 0.22$ nm which occurs for a relative humidity $= 0.1$ [8].

Assume the solids are squeezed together with an external pressure $p_0 = F_0/A_0$. If ΔA is the surface area occupied with water, then the attractive capillary force acting on the upper solid is $F_{\rm ad} = p_{\rm K}\Delta A$. In a mean-field type of approach we replace the nonuniform adhesive pressure from the capillary bridges with a uniform pressure $p_{\rm ad} = F_{\rm ad}/A_0$. To determine the contact area, and the probability distribution $P(u) = \langle\delta[u - u(x,y)]\rangle$ of interfacial separation, we assume that the solids are squeezed together with the pressure $p = p_0 + p_{\rm ad}$. Note that the applied pressure p_0 is negative during pull-off.

We use the Persson contact mechanics theory [5,39–41] to calculate $P(u)$. We assume that water occupies all the interfacial non-contact surface area where the separation $u(x,y) < d_{\rm K}$. We obtain the work of adhesion by integrating $p_0(\bar{u})$ as a function of the (average) separation $\bar{u}$ from the equilibrium separation (where $p_0 = 0$, and where $p_{\rm ad}$ is balanced by the repulsive pressure from the area of real contact) to infinite separation (where again $p_0 = 0$). For more details see Ref. [7].

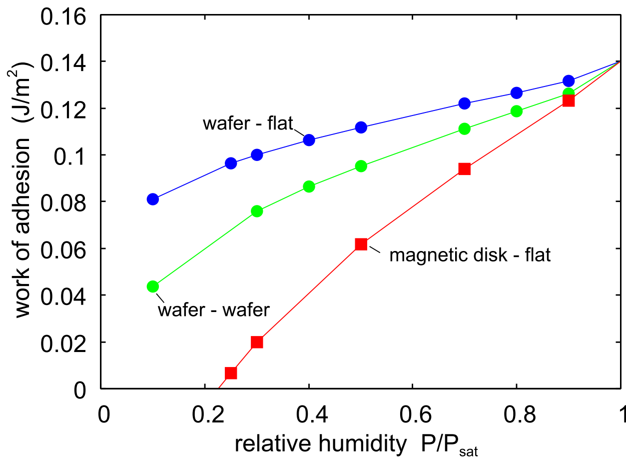

Fig. 7 The work of adhesion as a function of the relative humidity RH $= P/P_{\mathrm{sat}}$ (where P is the water partial pressure and P_{sat} the saturated water partial pressure). Results are shown for the contact between a perfectly flat surface and the wafer surface (blue symbols), and between two wafer surfaces (green symbols) using the fitted line power spectrum in Fig. 4. The red symbols are the results for the magnetic disk against a flat

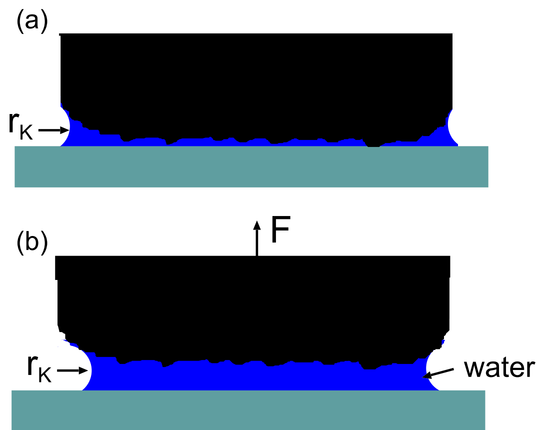

Fig. 8 When the Kelvin length, which equals $2r_{\mathrm{K}}$ for wetting liquids, becomes much larger than the surface roughness amplitude, the work of adhesion approach $w = 2\gamma$, where γ is the water surface tension

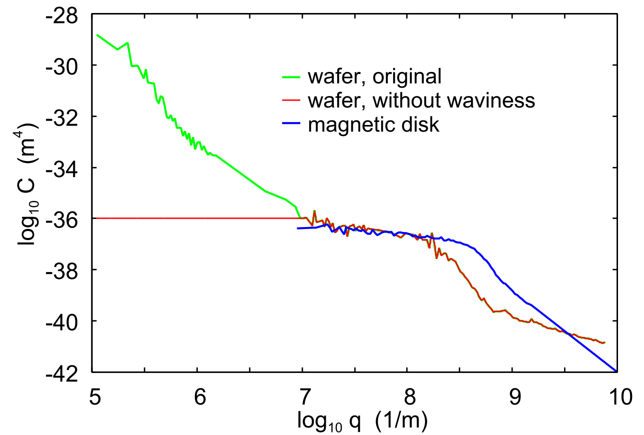

Fig. 9 The surface roughness power spectrum of the wafer surface (green line) and of the same surface after removing the waviness (red). The blue line is the power spectrum of a magnetic disk

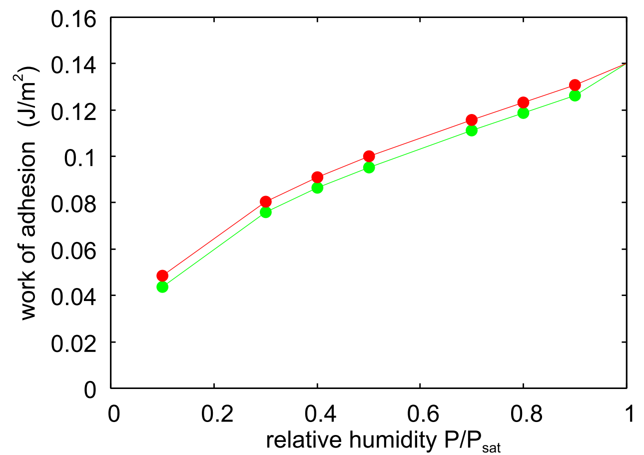

Fig. 10 The work of adhesion calculated with and without long-wavelength roughness as a function of the relative humidity RH $= P/P_{\mathrm{sat}}$ (where P is the water partial pressure and P_{sat} the saturated water partial pressure). Results are shown for the contact between two wafer surfaces (green symbols) using the green line power spectra shown in Fig. 9. The red symbols are for the contact between two wafer surfaces after removing the waviness, i.e. using the red line power spectrum in Fig. 9

5 Numerical results

We will now study the work of adhesion assuming thermal (kinetic) equilibrium with the water vapor. We consider the contact between two wafer surfaces and also the contact between a wafer surface and a perfectly flat surface, which can also be interpreted as the contact between two wafer surfaces with the combined power spectra reduced by a factor of 2 (or the rms-roughness of both surfaces reduced by a factor of $\sqrt{2}$).

Figure 7 shows the work of adhesion as a function of the relative humidity RH $= P/P_{\mathrm{sat}}$ (where P is the water partial pressure and P_{sat} the saturated water partial pressure). Results are shown for the contact between two wafer surfaces (green symbols) and for the contact between a wafer surface and a perfectly flat counter surface (blue symbols). Also shown is the contact between the magnetic disk and a flat surface (red symbols).

Note that no capillary adhesion occurs when the surfaces are fully immersed in water; but, when the relative humidity RH < 1, capillary adhesion occurs and the capillary bridges have a finite (maximal) height. The higher the relative humidity, the higher the height of these capillary bridges, and the longer the distance needed to break from these capillary bridges. In particular, when the relative humidity is very close to 1, the Kelvin length d_{K} and becomes much larger than surface

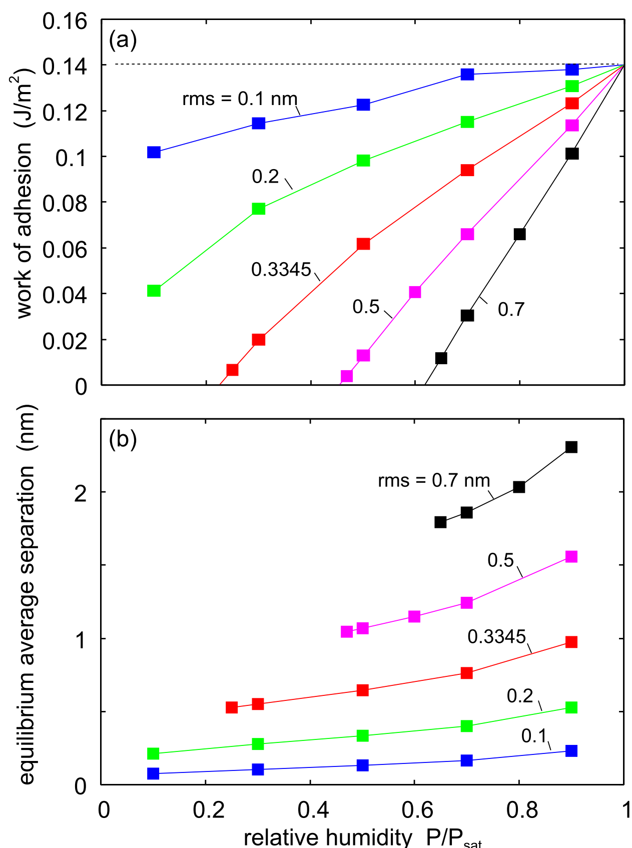

Fig. 11 The work of adhesion (**a**) and the average surface separation at equilibrium (**b**), as a function of the relative humidity RH $= P/P_{\mathrm{sat}}$ (where P is the water partial pressure and P_{sat} the saturated water partial pressure). Results are shown for five different surfaces with the rms roughness amplitudes $h_{\mathrm{rms}} = 0.1$, 0.2, 0.3345, 0.5 and 0.7 nm. The surface roughness power spectra are obtained by scaling the roughness of the magnetic disk with appropriate scaling factors. The red data ($h_{\mathrm{rms}} = 0.3345$ nm) is assuming the power spectrum of the magnetic disk shown in Fig. 9 (red line)

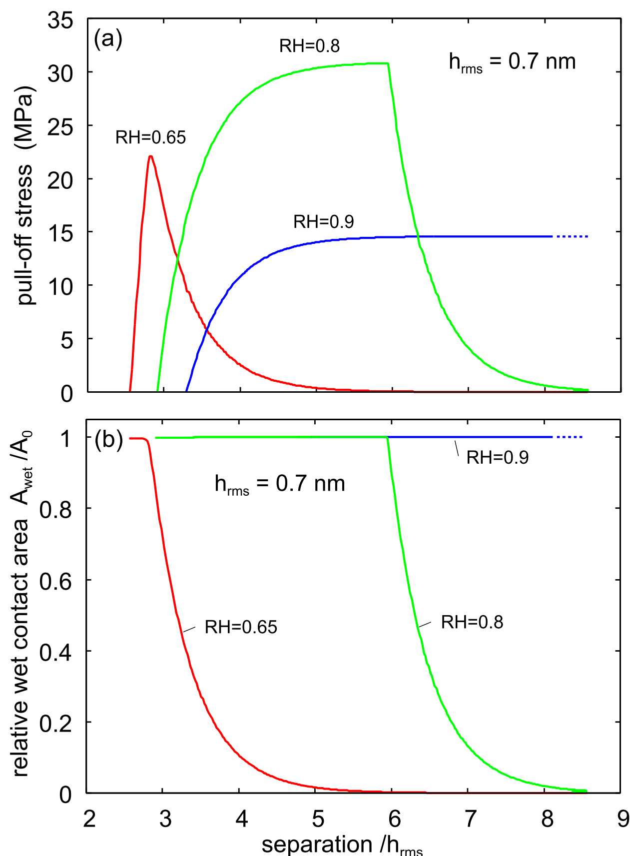

Fig. 12 a The force per unit surface area (pull-off stress) needed to separate the surfaces for the $h_{\mathrm{rms}} = 0.7$ nm surface for the relative humidity's RH = 0.65, 0.8 and 0.9. **b** The relative contact area covered by water as a function of the (average) surface separation (in units of the rms surface roughness h_{rms}) during pull-off. It is assumed that the system is in thermal equilibrium with the water vapor, which will be the case if the pull-off occurs slowly enough

roughness amplitude. In this case, the surfaces need to be separated by $\approx d_{\mathrm{K}}$ before the capillary bridges are broken (see Fig. 8). Further, the work of adhesion is $w \approx p_{\mathrm{K}} d_{\mathrm{K}}$, and since the Laplace pressure for a meniscus is $p_{\mathrm{K}} = \gamma / r_{\mathrm{K}}$ and since $d_{\mathrm{K}} = 2r_{\mathrm{K}}$ for a wetting liquid, this gives $w \approx (\gamma / r_{\mathrm{K}}) \times (2r_{\mathrm{K}}) = 2\gamma$. In other words, the work of adhesion approaches 2γ as the water partial pressure P approaches P_{sat} (i.e., as RH $\to 1$.)

To help show that the short wavelength roughness matters most for the capillary adhesion we have calculated the work of adhesion for the case where we remove the waviness part of the surface roughness. (The red line in Fig. 9 shows the surface roughness power spectra used in the calculation.) Fig. 10 shows the work of adhesion as a function of the relative humidity for the contact between two wafer surfaces (green symbols) using the full surface roughness power spectrum. The red symbols are for the contact between two wafer surfaces after removing the waviness.

Note that removing the waviness part of the roughness has only a small influence on the result. This is due to the roll-off region separating the long-wavelength (waviness) roughness from the short wavelength roughness. This is also reflected in the rms-slope which is $\approx 4 \times 10^{-4}$ for the (low resolution) measurement on the 80 μm surface area and ≈ 0.2 for the (high resolution) measurement on the 0.2 μm surface area.

To further illustrate how short wavelength roughness determines the work of adhesion, we have repeated the calculation using the roughness power spectrum of the magnetic disk from a hard disk drive. This power spectrum is shown in Fig. 9 (blue line). This roughness power spectrum was obtained from an AFM topography image collected over a 1 μm $\times$ 1 μm area. This magnetic disk is similar to the one described Section 2.4.3.1 of Ref. [9]. While still very smooth, it has about twice the rms roughness as the silicon surface over a 1 μm $\times$ 1 μm area ($h_{\mathrm{rms}} \approx 0.33$ nm versus ≈ 0.14 nm), and a higher rms slope ($\xi \approx 0.28$ versus ≈ 0.20), but much smaller long wavelength roughness (not shown).

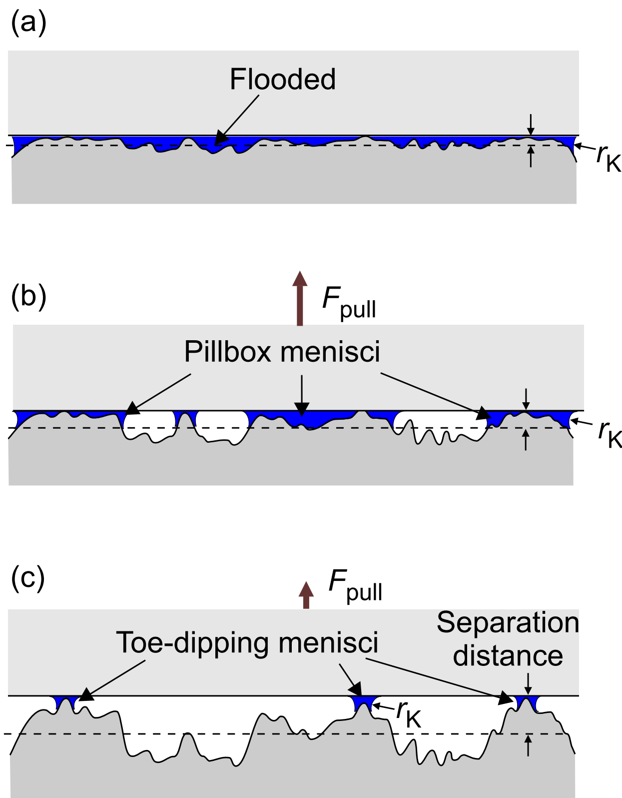

Fig. 13 Illustration of both the elastic deformation of a rough surface pressed against a rigid smooth surface and the different wetting regimes that form at this contacting interface at different separation distances due to capillary condensation. Note that amount of elastic deformation is greatly exaggerated. The terms for the different wetting regimes (flooded, pillbox, toe-dipping) are from Refs. [9,12]. Note that the term "pillbox" is used to describe those menisci with a shape similar to old fashion, cylindrical shaped boxes used to store pills which had a small height to diameter ratio

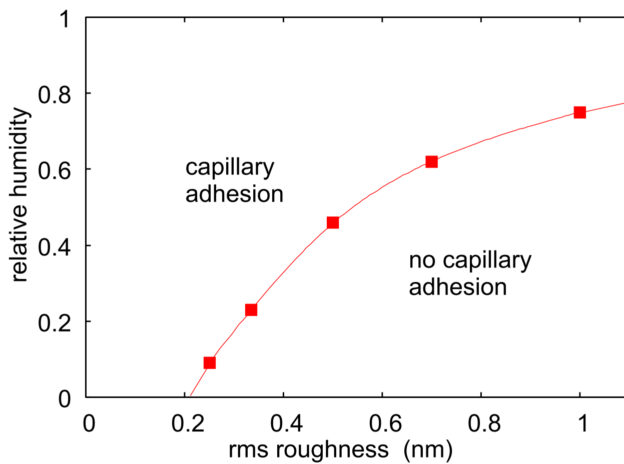

Fig. 14 Boundary line in the RH $-$ $h_{\rm rms}$ plane between wafers exhibiting capillary adhesion sufficient to overcome the elastic deformation force and collapse the interface and wafers with insufficient capillary adhesion to lead to direct bonding

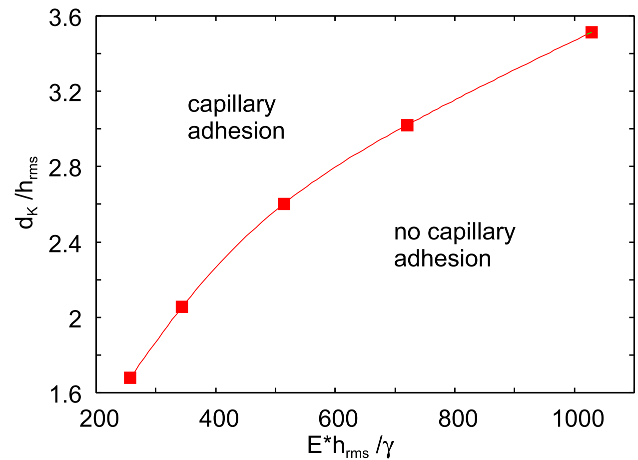

Fig. 15 Boundary line in the $d_{\rm K}/h_{\rm rms} - E^*h_{\rm rms}/\gamma$ plane between wafers exhibiting capillary adhesion sufficient to overcome the elastic deformation force and collapse the interface and wafers with insufficient capillary adhesion to lead to direct bonding

(Thus the condition $\xi << 1$ needed for the theory to be accurate is approximately satisfied.) The work of adhesion of the magnetic disk against a flat is shown in Fig. 7. Due to the larger short wavelength roughness, this surface has much lower values of the work of adhesion.

We now study how scaling the power spectrum by different factors affects the capillary adhesion. Figure 11a shows the work of adhesion and Fig. 11b the average surface separation at equilibrium, as a function of the relative humidity RH $= P/P_{\rm sat}$. The average separation is defined as the volume of the non-solid portion of the interface (wet and dry) divided by the nominal area of the interface. Results are shown for five different surfaces with the power spectrum of the magnetic disk surface scaled so that the the rms roughness amplitudes are $h_{\rm rms} = 0.1$, 0.2, 0.33, 0.5 and 0.7 nm. Again, it is assumed that the system is in equilibrium with the water vapor.

Next we consider how the force per unit area (pull-off stress) varies as the two surfaces are pulled apart (with the surfaces parallel) after contact. Figure 12a shows the pull-off stress as a function of separation distance for the $h_{\rm rms} = 0.7$ nm surface for the relative humidities RH $= 0.65$, 0.8 and 0.9. Note that the areas under these curves yields the work of adhesion, and that, for the three studied humidities, the highest work of adhesion is for the highest humidity RH $= 0.9$, but the pull-off stress (during uniform separation) is highest for RH $=$ 0.8. Figure 12b shows the relative contact area covered by water as a function of the average surface separation (in units of the rms surface roughness $h_{\rm rms}$) during pull-off.

The shapes of the curves in Fig. 12 can be understood in terms of the schematic diagrams in Fig. 13, which illustrate both elastic deformation of a rough surface when pressed against a smooth, rigid surface and the different wetting menisci that form due capil-

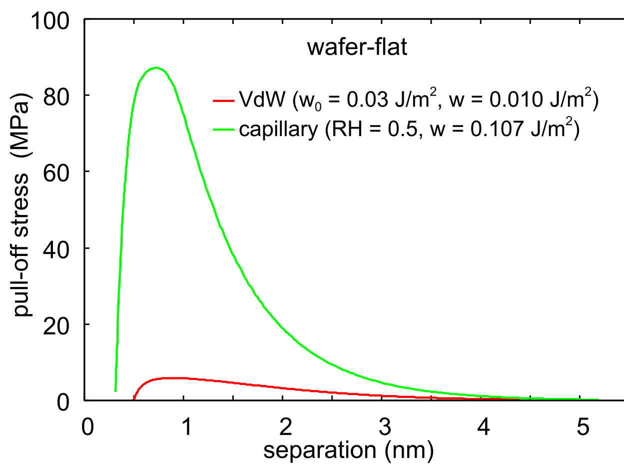

Fig. 16 The force per unit surface area (pull-off stress) needed to separate the surfaces for the Si wafer-flat interface in the dry state assuming VdW interaction between the surfaces (red line), and due to capillary bridges (green line) (the relative humidity RH = 0.5). For the VdW interaction we have assumed that the adhesive pressure depends on the surface separation as $\propto u^{-3}(x, y)$ and that the work of adhesion between to ideally smooth, solid surfaces is $w_0 = 0.03\ \mathrm{J/m^2}$

lary condensation of water vapor. Figure 13a shows the situation where the contact interface is flooded with the condensed water (at high enough humidity) and the capillary adhesion force $F_a = p_K A_0$ is balanced the elastic repulsive force; this situation corresponds to the leftmost point of the curves in Fig. 12. When an increasing pull-off force $F_{\rm pull}$ is applied to separate the surfaces, the interface remains flooded ($A_{\rm wet}/A_0 = 1$ part of the curves in Fig. 12b) until parts of the interface become separated by distances greater than d_K and dry voids start to appear in the interface. This results in the kinks in the curves in Fig. 12b where $A_{\rm wet}/A_0$ becomes < 1. At first the interface is wet mainly by large area, pillbox shaped menisci (Fig. 13b), but as the surfaces are further separated, these pillbox menisci shrink to toe-dipping menisci, and the capillary adhesion decreases as the wet area decreases until only a few toe-dipping menisci remain at the last contacting asperities (Fig. 13c). Figure 13 also illustrates how, as the loading force on the contacting interface is reduced, the surface roughness elastically relaxes back to its unstressed topography.

In order to achieve solid-solid contact over a large area (as shown in Fig. 13a) the right combination of conditions have to occur for the capillary adhesive force to be large enough to overcome the elastic repulsive force in order to collapse the interface, a precursor step to achieving direct bonding between two wafers. Figure 14 shows the boundary line in the RH$-h_{\rm rms}$ plane between wafers exhibiting capillary adhesion sufficient to collapse a hydrophilic interface and those situations where the capillary adhesion is insufficient at any separation distance to overcome the elastic repulsive deformation force from the contacting asperities. As expected, smoother surfaces with a low value of $h_{\rm rms}$ can be collapsed with a low value RH, while rougher surfaces require higher humidity. (For example, for $h_{\rm rms} = 1$ nm a relative humidity of RH > 0.75 is needed in order for capillary adhesion to induce interfacial collapse.)

For a given shape of the surface roughness power spectrum, the capillary adhesion theory enters only through the parameters d_K, $h_{\rm rms}$, E^* and the liquid surface tension γ. From these parameters one can only construct two (independent) dimensionless parameters, namely $d_K/h_{\rm rms}$ and $E^* h_{\rm rms}/\gamma$. Hence the boundary line separating capillary adhesion from non-adhesion must depend on only these parameters. In Fig. 15 we show the boundary line in the $d_K/h_{\rm rms} - E^* h_{\rm rms}/\gamma$ plane separating wafers exhibiting capillary adhesion from those situations with insufficient capillary adhesion to collapse the interface. As expected reducing the elastic modulus E^* or the root-mean-square roughness amplitude $h_{\rm rms}$, or increasing liquid surface tension γ result in capillary adhesion prevailing to smaller $d_K/h_{\rm rms}$ or smaller relative humidity.

Next, let us address the role of the van der Waals interaction in wafer bonding. In Fig. 16 we compare pull-off stress as a function of the (average) surface separation for the wafer-flat contact for the dry contact, with only the VdW interaction between the surfaces (red line), with the capillary case (green line) for relative humidity RH = 0.5. For the VdW interaction we have assumed that the adhesive pressure depends on the surface separation as $\propto u^{-3}(x, y)$ and that the work of adhesion for ideally smooth surfaces is $w_0 = 0.03\ \mathrm{J/m^2}$ (see Ref. [10] for details of the model). For the dry case the work of adhesion (the area under the stress-separation curve) is $w \approx 0.01\ \mathrm{J/m^2}$, and for capillary adhesion is about 10 times higher. This is similar to the difference in binding strength for the perfect sphere-flat configuration (Bradley case), but in that case the result does not depend on the humidity, in contrast to wafer bonding. It is also interesting to note that for the adhesion between hard particles with big surface roughness (such as mineral particles produced by fracture, e.g. crunched stone) the capillary force is typically ~ 100 times bigger than the van der Waals adhesion force [13, 14].

6 Discussion

The breaking the adhesive bond between two surfaces is almost never uniform, but occurs instead by interfacial crack propagation. The onset of this crack propagation, however, is determined by the work of adhesion rather than the maximum pull-off stress during uniform separation. Since the interfacial collapse that occurs during the direct bonding between two wafers is just the reverse process of crack propagation, the work of adhesion is the most relevant parameter for the direct bonding process.

The work of adhesion depends not only on the interaction force but on the distance over which it acts. Thus strong adhesion typically results from “long bonds”

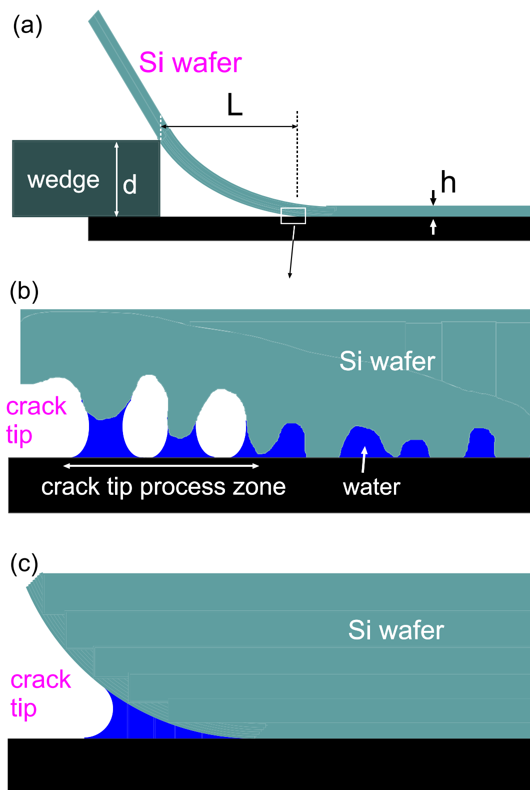

Fig. 17 **a** The cantilever bending test methodology to determine the work of adhesion w for a thin elastic sheet bound to a substrate (black) here assumed to be rigid. For two wafers in contact the work of adhesion $w = 3Ed^2h^3/(16L^4)$. **b** The crack tip process zone for a stationary crack (thermal equilibrium). The work of adhesion is the work to separate the surfaces from the equilibrium (bonding) position (to the right of the crack tip) to the fully separated (non-bonding) state (to the left of the crack tip) where no capillary bridges occur between the surfaces. **c** The work of adhesion is maximal for the case of smooth surfaces where the capillary contribution to the work of adhesion equals 2γ, where γ is the surface tension of water

rather than "strong bonds" [44]. For the case of capillary adhesion, this depends mainly on d_K and hence on the relative humidity. When the humidity increases, the distance needed to break a capillary bridge increases, and this is more important than the magnitude of the force the capillary menisci exert on the surfaces. This can be seen in Fig. 12a which shows that for the three RH used, the maximum force takes its highest value for the relative humidity RH = 0.8, but the work of adhesion increases continuously with increasing humidity and is larger for 0.9 than for 0.8 (Fig. 11).

We note that for small and elastically stiff solid objects the bond-breaking during pull-off does not occur by interfacial crack propagation but occurs uniformly in the nominal contact area [43,45]. In this case the maximum pull-off force will occur for a relative humidity < 1 (which depends on the surface roughness) as typically observed in AFM pull-off experiments [47].

Figure 17a shows a typical experiment used to determine the work of effective adhesion w_0 for a thin elastic sheet (e.g. a silicon wafer) bound to a substrate here assumed to be rigid. The work of adhesion w_0 can be determined by minimizing the total energy which has a positive contribution from bending the sheet and a negative contribution from the binding of the sheet to the substrate, leading to the equation $w_0 = 3Ed^2h^3/(16L^4)$ (here we have assumed two bound silica wafers, see Ref. [29]). The work of adhesion w_0 depends on the complex separation processes occurring in some region close to the crack tip (the crack-tip process zone) where the capillary bridges are broken. (When determining w_0, we assume stationary contact and thermal equilibrium.) Thus the work of adhesion is the work to adiabatically separate the surfaces from the equilibrium bonding position (to the right of the crack tip in Fig. 17) to the fully separated non-bonding state (to the left of the crack tip) where no capillary bridges are present between the surfaces. The work of adhesion is maximal for the case of smooth, flooded surfaces where the capillary contribution to the work of adhesion equals 2γ, where γ is the surface tension of water.

Next we consider other factors that can contribute to the work of adhesion during direct wafer bonding. One can distinguish several stages in wafer bonding [30]:

Stage 1 - Prior to wafer bonding, the surfaces need to be cleaned and "activated". For silicon wafers, two surface activation methods are used: exposure to oxygen plasma or wet chemical surface activation. This step ensures that the silicon oxide surfaces are covered with a high density Si-OH groups, that not only make the surface hydrophilic, but are also necessary for strong covalent bonds to form during the annealing stage.

Stage 2 - The interface is collapsed using the hydrophilic bonding process discussed in this paper, where the adhesion originates from the Laplace pressure in the capillary menisci from the condensation of water vapor.

Stage 3 - To form strong covalent bonds across the solid-solid interface, the surface is annealed to typically $T \approx 800°$C. This annealing cycle removes water from the interface and promotes covalent oxide bonds forming across the interface, strongly bonding the wafers together. During annealing, a condensation polymerization reaction occurs to produce covalent high strength bonding:

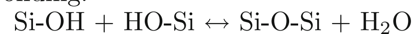
Si-OH + HO-Si $\leftrightarrow$ Si-O-Si + H_2O

This reaction is reversible up to 400°C, but at higher temperatures the released water is able to diffuse into the bulk silicon, releasing hydrogen via

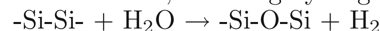
-Si-Si- + $H_2O \rightarrow$ -Si-O-Si + H_2

(This hydrogen gas is the primary cause of annealing voids.)

This picture has some similarities to the binding of cellulose fibers in paper. To bind the fibers the surfaces must first be chemically "activated" to increase the surface energy and make the surfaces more hydrophilic. During drying of wet fibers water capillary bridges pull the fibers into such close contact that hydrogen bonds can form between hydroxyl groups on adjacent cellulose

fibers. In addition, interdiffusion of fibrils between the (in the wet state) gel-like surface layers on the cellulose fibers affect the bonding strength between the fibers in the dry state [48].

We now consider the extent that plastic deformation might impact the work of adhesion. For the case of maximal height of the water film ($d_K = 0.44$ nm for RH = 0.1 and $d_K = 9.59$ nm for RH = 0.9) the corresponding squeezing pressures from the condensed water menisci are $p \sim 2\gamma/d_K \approx -319$ MPa and ≈ -15 MPa, respectively. However, due to the surface roughness, the area of solid-solid contact is very small, as contact only occurs at the summits of the asperities resulting in relatively high contact pressures occurring over these areas of contact. These contact pressures are of the order of 25 GPa for the roughest surface studied in Fig. 11 (with $h_{\rm rms} = 0.7$ nm). This stress is similar to the yield stress $\sim$ 10 GPa of silica at the nanoscale [49] and is sufficient to cause plastic deformation to occur, increasing slightly the area of solid-solid contact area and its contribution to the work of adhesion. The plastic deformation may be further increased during the heating cycle, as increased temperature lowers of the yield strength. At high temperatures of $800 - 1400°$C silicon oxide flows slightly (i.e., plastically deforms), filling interfacial voids and helping to form a "perfect" bond.

In addition to plastic flow we note that with increasing pressure silicon undergoes various phase transformations whose stress thresholds are dependent on the loading/unloading conditions [50]. In loading at a pressure of $10 - 12$ GPa the original diamond structure of silicon transforms into a denser β-tin (metallic) phase, accompanied by a 22% volumetric reduction. Hence the region below the SiO_2 film may not deform just elastically but more complex structural changes may occur.

The study presented above is valid for other elastically stiff materials ($E^* \sim 10^{11}$ Pa or higher) with very smooth surfaces, where the water contact angle is well below 90°, giving hydrophilic interfaces. This includes most ceramic materials like SiC, CrN and TiN which have water contact angles of order $\sim 30°$. For elastically softer materials like glassy polymers with hydrophilic interfaces (e.g. as a result of exposure to oxygen plasma) capillary adhesion will manifest itself for much larger surface roughness than for the silica surfaces studied above.

For very soft materials such as rubber, the capillary adhesion can have a major influence on the area of real contact, as predicted and observed for wiper blades on glasses surface [7,51]. In this case, as the water is removed by wiping and evaporation, as a function of time a high friction peak, with a friction considerably higher than the dry one, may be observed. Experiments [51] have shown that in the tacky regime the attraction from water capillary bridges between the rubber and the glass substrate pull the rubber into close contact with the substrate so that the area of real contact is even larger in the tacky regime than for the perfectly dry contact. Similar effects have been observed for the human skin [52,53].

7 Summary and conclusions

We have studied the influence of surface roughness and humidity on the work of adhesion for the case of hydrophilic wafer bonding. In agreement with experiments, we find that the surfaces with roughness greater than $\sim$ 1 nm rms amplitude (when measured over a surface area of order 1 μm$\times$1 μm) will not bond under typical conditions unless the humidity is very close to the saturation level (i.e., relative humidity RH > 0.8). For any given surface roughness, the force needed to separate two solids with nominal flat surfaces takes a maximum for some relative humidity between 0 and 1 assuming the solids are separated with their surfaces parallel. Also, since bond breaking occurs non-uniformly in the form of interfacial crack propagation, the pull-off force is determined by the work of adhesion, which increases continuously with the humidity and reaches the value $2\gamma \approx 0.14$ J/m^2 as RH $\to 1$. We have shown that in the case of hydrophilic bonding of silicon wafers, the long-wavelength roughness (usually denoted waviness) has a negligible influence on the strength of wafer bonding (the work of adhesion) due to capillary bridges.

We thank Mark Spearing (University of Southampton) for useful communication about wafer bonding. We thank Robert Carpick (University of Pennsylvania) and Bart Weber (University of Amsterdam) for comments on the text. Part of this work (AFM imaging) was performed at the Stanford Nano Shared Facilities (SNSF) supported by the National Science Foundation under award ECCS-2026822.

Author contributions

All authors contributed equally to the paper.

Funding Open Access funding enabled and organized by Projekt DEAL.

Data availability This manuscript has no associated data or the data will not be deposited. [Authors' comment: All numerical data generated during this study are available on request.]

Declarations

Conflict of interest The authors report no declarations of interest.

Open Access This article is licensed under a Creative Commons Attribution 4.0 International License, which permits use, sharing, adaptation, distribution and reproduction in any medium or format, as long as you give appropriate credit to the original author(s) and the source, provide a link to the Creative Commons licence, and indicate if changes were made. The images or other third party material in this article are included in the article's Creative Commons licence, unless indicated otherwise in a credit line to the material. If material is not included in the article's Creative Commons

licence and your intended use is not permitted by statutory regulation or exceeds the permitted use, you will need to obtain permission directly from the copyright holder. To view a copy of this licence, visit http://creativecommons.org/licenses/by/4.0/.

References

1. A. Tiwari, J. Wang, B.N.J. Persson, Adhesion paradox: Why adhesion is usually not observed for macroscopic solids. Phys. Rev. E **102**, 042803 (2020)
2. B.N.J. Persson, O. Albohr, U. Tartaglino, A.I. Volokitin, E. Tosatti, On the nature of surface roughness with application to contact mechanics, sealing, rubber friction and adhesion. J. Phys.: Condens. Matter **17**, R1 (2004)
3. B.N.J. Persson, Adhesion between an elastic body and a randomly rough hard surface. The European Physical Journal E **8**, 385 (2002)
4. B.N.J. Persson, E. Tosatti, The effect of surface roughness on the adhesion of elastic solids. J. Chem. Phys. **115**, 5597 (2001)
5. B.N.J. Persson, Contact mechanics for randomly rough surfaces. Surf. Sci. Rep. **61**, 201 (2006)
6. M. Binggeli, C.M. Mate, Influence of capillary condensation studied by force microscopy of water on nanotribology. Appl. Phys. Lett. **65**, 415 (1994)
7. B.N.J. Persson, Capillary adhesion between elastic solids with randomly rough surfaces. J. Phys.: Condens. Matter **20**, 315007 (2008)
8. J.N. Israelachvili, Intermolecular and Surface Forces, Thrid Edition, Academic Press (2011)
9. C.M. Mate, R.W. Carpick, *Tribology on the Small Scale: A Modern Textbook on Friction, Lubrication, and Wear*, 2nd edn. (Oxford University Press, Oxford, 2019)
10. B.N.J. Persson, M. Scaraggi, Theory of adhesion: Role of surface roughness. J. Chem. Phys. **141**, 124701 (2014)
11. Rostami, J.L. Streator, Study of liquid-mediated adhesion between 3D rough surfaces: A spectral approach Tribology International, **84**, 36 (2015)
12. M.J. Matthewson, H.J. Mamin, Liquid Mediated Adhesion of Ultra-Flat Solid Surfaces MRS Online Proceedings Library (OPL) **119**, 87 (2011)
13. B.N.J. Persson, J. Biele, On the stability of spinning asteroids. Tribol. Lett. **70**, 34 (2022)
14. B.N.J. Persson, Influence of humidity on the binding of stone fragments via capillary bridges. Europhys. Lett. **137**, 46001 (2022)
15. F. Cassin, R. Hahury, T. Lanon, S. Franklin, B. Weber, The nucleation, growth, and adhesion of water bridges in sliding nano-contacts. J. Chem. Phys. **158**, 224703 (2023)
16. C. Xiao, L. Peng, C. Leriche, F.C. Hsia, B. Weber, S. Franklin, Capillary adhesion governs the friction behavior of electrochemically corroded polycrystalline diamond. Carbon **205**, 345 (2023)
17. L. Peng, F.C. Hsia, S. Woutersen, M. Bonn, B. Weber, D Bonn Nonmonotonic friction due to water capillary adhesion and hydrogen bonding at multiasperity interfaces. Phys. Rev. Lett. **129**, 256101 (2022)
18. F.C. Hsia, C.C. Hsu, L. Peng, F.M. Elam, C. Xiao, S. Franklin, D. Bonn, B Weber Contribution of capillary adhesion to friction at macroscopic solid-solid interfaces. Phys. Rev. Appl. **17**, 034034 (2022)
19. F.C. Hsia, S. Franklin, P. Audebert, A.M. Brouwer, D. Bonn, B. Weber, Rougher is more slippery: how adhesive friction decreases with increasing surface roughness due to the suppression of capillary adhesion. Phys. Rev. Res. **3**, 043204 (2021)
20. R.W. Liefferink, B. Weber, D. Bonn, Ploughing friction on wet and dry sand. Phys. Rev. E **98**, 052903 (2018)
21. A. Fall, B. Weber, M. Pakpour, N. Lenoir, N. Shahidzadeh, J. Fiscina, C. Wagner, D. Bonn, Sliding friction on wet and dry sand. Phys. Rev. Lett. **112**, 175502 (2014)
22. L. Peng, C.C. Hsu, C. Xiao, D. Bonn, B. Weber, Controlling Macroscopic Friction through Interfacial Siloxane Bonding. Phys. Rev. Lett. **131**, 226201 (2023)
23. J.B. McClimon, Z. Li, D. Goldsby, I. Szlufarska, R.W. Carpick, The Effects of Humidity on the Velocity-Dependence and Frictional Ageing of Nanoscale Silica Contacts, (preprint) https://doi.org/10.21203/rs.3.rs-3348903/v1
24. F.W. DelRio, M.L. Dunn, L.M. Phinney, C.J. Bourdon, M.P. de Boer, Rough surface adhesion in the presence of capillary condensation. Appl. Phys. Lett. **90**, 163104 (2007)
25. R.S. Bradley, The cohesive force between solid surfaces and the surface energy of solids. Philos. Magn. Ser. **13**, 853 (1932)
26. E. Navarro, Y. Brechet, A. Barthelemy, I. Radu, J.-P. Raskin, T. Pardoen, Adhesion and separation models for direct hydrophilic bonding. J. Appl. Phys. **117**, 085305 (2015)
27. C. Gui, M. Elwenspoek, N. Tas, J.G.E. Gardeniers, The effect of surface roughness on direct wafer bonding. J. Appl. Phys. **85**, 7448 (1999)
28. A. Usenko, Humidity effects on substrate bonding for silicon-on-glass. ECS Trans. **35**, 111 (2011)
29. A. Plössl, R. Scholz, J. Bagdahn, H. Stenzel, K.N. Tu, U. Gösele, In: H.R. Huff, H. Tsuya, U. Gösele (Eds.), Proc. 8th Int. Symp. on Silicon Material Science and Technology, vol. 2, The Electrochemical Society, Pennington, NJ, pp. 1361-1372 (San Diego, CA) (1998)
30. V. Masteika et al., A review of hydrophilic silicon wafer bonding. ECS J. Solid State Sci. Technol. **3**, Q42 (2014)
31. K.T. Turner, S.M. Spearing, Mechanics of direct wafer bonding. Proc. R. Soc. A **462**, 171 (2006)
32. N. Miki, S.M. Spearing, Effect of nanoscale surface roughness on the bonding energy of direct-bonded silicon wafers. J. Appl. Phys. **94**, 6800 (2003)
33. K.T. Turner, S.M. Spearing, W.A. Baylies, M. Robinson, R. Smythe, Effect of Nanotopography in Direct Wafer Bonding: Modeling and Measurements. IEEE Trans. Semicond. Manuf. **18**, 289 (2005)
34. D.J. Cole, M.C. Payne, G. Csanyi, S.M. Spearing, L.C. Ciacchi, Development of a classical force field for the oxidized Si surface: Application to hydrophilic wafer bonding. J. Chem. Phys. **127**, 204704 (2007)
35. F. Rieutord, B. Bataillou, H. Moriceau, Dynamics of a bonding front. Phys. Rev. Lett. **94**, 236101 (2005)
36. M.M. Kohonen, N. Maeda, H.K. Christenson, Kinetics of Capillary Condensation in a Nanoscale Pore. Phys. Rev. Lett. **82**, 4667 (1999)

37. A.L. Barabasi, H.E. Stanley, *Fractal Concept in Surface Growth* (Cambridge University Press, Cambridge, 1995)
38. B.N.J. Persson, On the Fractal Dimension of Rough Surfaces. Tribol. Lett. **54**, 99 (2014)
39. B.N.J. Persson, Theory of rubber friction and contact mechanics. J. Chem. Phys. **115**, 3840 (2001)
40. L. Afferrante, F. Bottiglione, C. Putignano, B.N.J. Persson, G. Carbone, Elastic contact mechanics of randomly rough surfaces: an assessment of advanced asperity models and Persson's theory. Tribol. Lett. **66**, 1 (2018)
41. A. Almqvist, C. Campana, N. Prodanov, B.N.J. Persson, Interfacial separation between elastic solids with randomly rough surfaces: Comparison between theory and numerical techniques. J. Mech. Phys. Solids **59**, 2355 (2011)
42. T.D.B. Jacobs, T. Junge, L. Pastewka, Quantitative characterization of surface topography using spectral analysis. Surf. Topogr.: Metrol. Prop **5**, 013001 (2017)
43. M.H. Müser et al., Meeting the Contact-Mechanics Challenge Tribol Lett **65**, 118 (2017)
44. B.N.J. Persson, On the mechanism of adhesion in biological systems. J. Chem. Phys. **118**, 7614 (2003)
45. B.N.J. Persson, Nanoadhesion. Wear **254**, 832 (2003)
46. M.H. Müser, B.N.J. Persson, Crack and pull-off dynamics of adhesive, viscoelastic solids. Europhys. Lett. **137**, 36004 (2022)
47. R.W. Carpick, J.D. Batteas, M.P. de Boer, See Fig. 32.8 in Scanning probe studies of nano-scale adhesion between solids in the presence of liquids and monolayer films, In: Handbook of Nanotechnology, 2nd Ed., (Ed. B. Bhushan) Springer. (Chapter in 1st Edition published 2004) (2006)
48. B.N.J. Persson, C. Ganser, F. Schmied, C. Teichert, Matter Adhesion of cellulose fibers in paper. J. Phys.: Condens. **25**, 045002 (2013)
49. A.J. Baker, S.B. Vishnubhotla, R. Chen, A. Martini, T.D.B. Jacobs, Origin of pressure-dependent adhesion in nanoscale contacts. Nano Lett. **22**, 5954 (2022)
50. See, T. Vodenitcharova, L.C. Zhang, A new constitutive model for the phase transformations in mono-crystalline silicon, International Journal of Solids and Structures **41**, 5411, and references therein (2004)
51. F. Deleau, D. Mazuyer, A. Koenen, Sliding friction at elastomer/glass contact: Influence of the wetting conditions and instability analysis. Tribol. Int. **42**, 149 (2009)
52. B.N.J. Persson, A.E. Kovalev, S. Gorb, Contact Mechanics and Friction on Dry and Wet Human Skin. Tribol. Lett. **50**, 17 (2012)
53. A.E. Kovalev, K. Dening, B.N.J. Persson, S.N. Gorb, Surface topography and contact mechanics of dry and wet human skin. Beilstein J. Nanotechnol. **5**, 1341 (2014)